Chin.J.Geochem.(2014)33:207–220
DOI: 10.1007/s11631-014-0680-4

LA-ICP-MS U-Pb zircon geochronology and Hf isotope, geochemistry and kinetics of the Daxigou anorthosite from Kuruqtagh block, NW China

YUAN Qian[1,2], CAO Xiaofeng[1,2], LÜ Xinbiao[1,2*], WANG Xiangdong[1], YANG Enlin[1], LIU Yuegao[1], RUAN Banxiao[1], LIU Hong[3], and MUNIR Mohammed Abdalla Adama[1]

[1] *Faculty of Earth Resources, China University of Geosciences, Wuhan 430074 ,China*

[2] *State Key Laboratory of Geological Processes and Mineral Resources, China University of Geosciences, Wuhan 430074, China*

[3] *Chengdu Center of China Geological Survey, Chengdu 610081, China*

[*] *Corresponding author, E-mail: sunshine24@foxmail.com*

Received January 10, 2014; accepted March 20, 2014

Abstract Kuruqtagh block is the best area for Precambrian geology in Xinjiang Autonomous Region, NW China, since it exposed complete Precambrian lithology units. The study of this ancient base will deepen the understanding of the Precambrian evolution of the Tarim Basin. In this paper, we studied the petrology, geochemistry, zircon LA-ICPMS U-Pb chronology and zircon Hf isotope of Daxigou anorthosite (DA) which is located at the northern margin of Tarim craton and discussed the rock formation, tectonic and geological significance. Zircons from the intrusions display oscillatory zoning and high Th/U ratios (0.39–1.35), implying their magmatic origin. Zircon LA-ICP-MS U-Pb dating results indicate that they formed during the Paleoproterozoic age with the weighted $^{206}Pb/^{238}U$ average age of 1818±9 Ma, which is significantly different from former's Neoproterozoic age, and is coincidentally identical with its associated syenite granite age within the error range. Studies on petrogeochemistry suggest that DA belongs to medium-sodium peraluminous alkaline type, rich in Pb, La, Th and LILE, and poor in HFSE (Gd, Nd, and Ta). The chondrite-normalized REE pattern is slightly to the right form. The average ∑REE is 317.2×10^{-6}; HREE show moderate fractionation [average LREE/HREE is 14.71, average $(La/Yb)_N$ is 24.77; average $(La/Sm)_N$ is 3.85, and average $(Gd/Yb)_N$ is 3.46]; and the δEu and δCe are not obvious. Their initial Hf isotope ratios and Hf two-stage model ages range from -6.6 to -4.43 and 2.63 to 2.74 Ga, respectively. Taken together, it is suggested that Daxigou anorthosite is a typical volcanic anorthosite and its primary magma could be contaminated by the partial melt Neoarchaean crust and mainly formed in the arc environment, which recoded the tectonic-magma activities response of the Tarim refers to the amalgamation of the supercontinent Columbia.

Key words Kuruqtagh block; Daxigou anorthosite; LA-ICP-MS zircon dating; Hf isotope; Paleoproterozoic

1 Introduction

The Tarim Craton (TC), one of the three largest cratons in China (i.e., TC, the North China Craton, and the South China Craton), records an important part of the early crustal evolutionary history of Northwest China and adjacent areas (Hu et al., 1997; Lu et al., 2008a, b; Demoux et al., 2009; Xiao and Kusky, 2009). The Kuruqtagh block outcrops on the northeast margin of the TC. It is the basement of the TC which was finally cratonized during the Tarimian Orogeny (Fig. 1A and B) (Gao et al., 1993; Li et al., 2002). The Kuruqtagh block comprises metamorphosed basement (from the Archaean to the Early Neoproterozoic) and sedimentary cover (from the Middle Neoproterozoic to the Phanerozoic) (Gao et al., 1993). Several tectono-thermal events from the latest Mesoproterozoic to Neochean have been distinguished in the study area.

However, most of which are mainly focused on the Neoproterozoic magmatism and tectonic evolution related to the break-up of Rodinia (e.g. Cao et al., 2010, 2011; Shu et al., 2010; Luo et al., 2007; Sun and Huang, 2007; Lu et al., 2008a, b; Zhang et al., 2007a, b, c, 2009, 2011; Xu et al., 2005, 2008, 2009; Zhu et al., 2008). Little is known about the pre-Neoprotero-

zoic magmatism and tectonic evolution of the TC.

Recently, a few research has revealed that the Paleoproterozoic magmatic-metamorphism activities are distributed in the area, but these are mainly model isotopic age data and LA-ICP-MS data from detrital zircon grains (Feng et al., 1995; Guo et al., 2003; Hu and Wei, 2006; Long et al., 2010; Shu et al., 2010) or about the metamorphic zircons (Lei et al., 2012). Until now none magmatic zircon isotopic ages have been reported in this area, which hinders a better understanding of tectonic evolution of the Precambrian cratons during the Archaean-Paleoproterozoic transitional time.

In this article, based on detailed field geology and petrological studies, we presented precise LA-ICP-MS zircon U-Pb geochronological, whole-rock geochemistry, and *in-situ* zircon Hf isotope composition data for the Daxigou anorthosite (DA) to define their emplacement ages, constrain their sources, evaluate their petrogenesis and geodynamic setting, and discuss the insights they provide for understanding the Paleoproterozoic geological evolution of the TC. Combined with the regional geological characteristics and geochronological data, implications for the Paleo-Mesoproterozoic assembly of Columbia were also discussed.

2 Regional geology

Kuruqtagh block is composed of two units: the basement which comprises the Archaean, Paleoproterozoic, Mesoproterozoic and Early Neoproterozoic lithologies, and the Middle Neoproterozoic to the Phanerozoic sedimentary cover (Cheng, 1994; Gao et al., 1993; Feng et al., 1995; Lu et al., 2008a, b) (Fig. 1B). Xinger and Xingdi faults are the main regional nearly EW-oriented structures.

Archaean rocks are well exposed in the center of Kuruqtagh block. The oldest rocks are known as the Tuogebulake Complex derived from TTG-type granites which yielded a zircon multigrain U-Pb TIMS age of 2582±11 Ma and a Pb-Pb zircon evaporation age of 2488±10 Ma (Lu Songnian, 1992). Paleoproterozoic rocks, mainly distributed at the western Kuruqtagh block, are known as Xingdi group consisting of older metamorphic mafic and felsic intrusions, high-grade metamorphic supracrustal rocks (schist and marble). An important metamorphic event was postulated to have affected the Archaean TTG suites and the overlying Paleoproterozoic sedimentary rocks by some previous workers (e.g. Feng, 1995; Lu et al., 2002), which took place at the end of the Paleoproterozoic and marked the formation of Archaean–Paleoproterozoic crystalline basement. Mesoproterozoic to Early Neoproterozoic low grade metamorphic rocks are widespread in the area including metamorphosed carbonate and clastic rocks, and granitoids (Feng et al., 1995; Lu et al., 2008a, b). Middle Neoproterozoic to Phanerozoic rocks consist of lower mafic dyke swarms, bimodal volcanics and upper fine sandstones, siltstones, shales, dark limestone and chert nodule-containing dolomite. The mafic dykes and bimodal volcanics formed in two stages: 820–744 Ma and 650–630 Ma (Zhang et al., 2007a, b, c, 2009; Xu et al., 2009, 2008; Zhu et al., 2008). Glacial deposits are also well exposed at the Late Neoproterozoic (Xu et al., 2008, 2009).

3 Field geology and petrography

The Daxigou complex located at the southern Xingdi fault in Kuruqtagh area (Fig. 1C) and is obvious controlled by its subsidiary fault. The coordinate of working area is 87°27′00″–87°31′00″E and 41°12′30″–41°15′30″N. This complex, which has the length of 2.1 km and width of 0.9 km (Fig. 2), is distributed from north-west to south-east and intrudes into the Archaean Tuogebulake Complex which is composed of amphogneiss and gneissic granite (Xia et al., 2010).

The intrusive complex investigated in this study is mainly composed of anorthosite and it is widely distributed in Daxigou deposit (Fig. 2). It is grayish white in color and exhibits coarse-grained granitic texture and blocky structure. The main mineral components are plagioclase (65%–70%), quartz (15%–20%), hornblende (5%–9%), magnetite (1%) and apatite (1%). The sampling locations of anorthosite were marked in Fig. 2.

Daxigou syenite granites (DSG) are mainly in the form of dike accompanying with the granodiorite in the periphery of Daxigou deposit (Fig. 2). It is noteworthy that some syenite granites are also found accompanying with the anorthosite, thus the syenite granites were also discussed to a better understanding of the studied anorthosite in the following. They are pinkish in color and show medium to coarse granitic textures. Their compositions include plagioclase (27%–45%), potassic feldspar (20%–25%), quartz (25%–30%), biotite (2%–5%), amphibole (1%–2%), and some accessory minerals (e.g. apatite, zircon).

4 Analytical methods

4.1 Zircon U-Pb dating

Zircon grains in the DA (DXG-16) were separated using conventional heavy liquid and magnetic techniques. Hand-picked zircon grains were mounted in epoxy blocks, polished to obtain an even surface, and cleaned with an acid bath before LA-ICP-MS analysis. The selection of zircon grains for isotopic

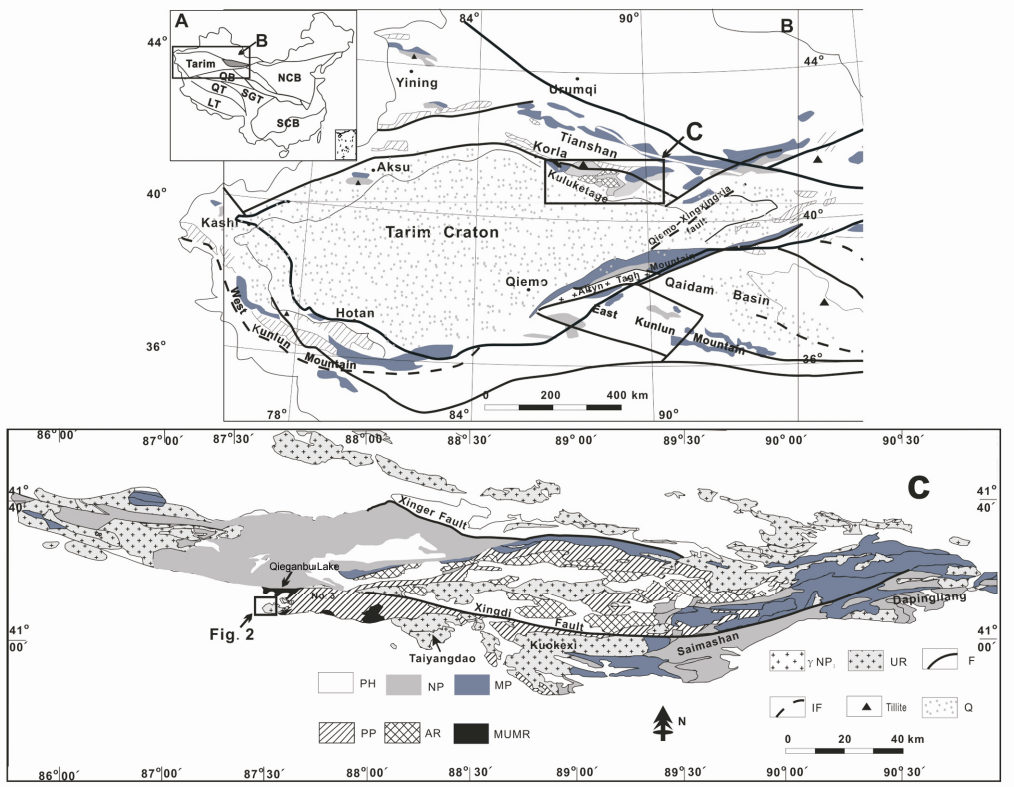

Fig.1A. Main tectonic domains of China (figure on the top left corner) and sketch map showing the Precambrian geology of the Tarim Craton and adjacent areas. B. Schematic geological map of Tarim Craton and adjacent areas. C. Schematic geological map of the Quruqtagh block on the northeast margin of the Tarim craton (Wang et al., 2007). NCB. North China Block; SCB. South China Block; SGT. Songpan–Ganzi Terrane; QB. Qaidam Basin; QT. Qiangtang Terrane; LT. Lhasa Terrane; PH. Phanerozoic rocks; NP. Neoproterozoic rocks; MP. Mesoproterozoic rocks; PP. Palaeoproterozoic rocks; AR. Archaean rocks; MUMR. Mafic-ultramafic rocks; γNP_1. Early Neoproterozoic granitoids; UR. unclassified granitoid rocks; F. faults; IF. inferred faults; Tillite. Nanhua and Sinian tillite; Q. Quaternary desert and sedimentary deposits; AT Mt. Altyn Tagh Mountains (Lu et al., 2008 a, b).

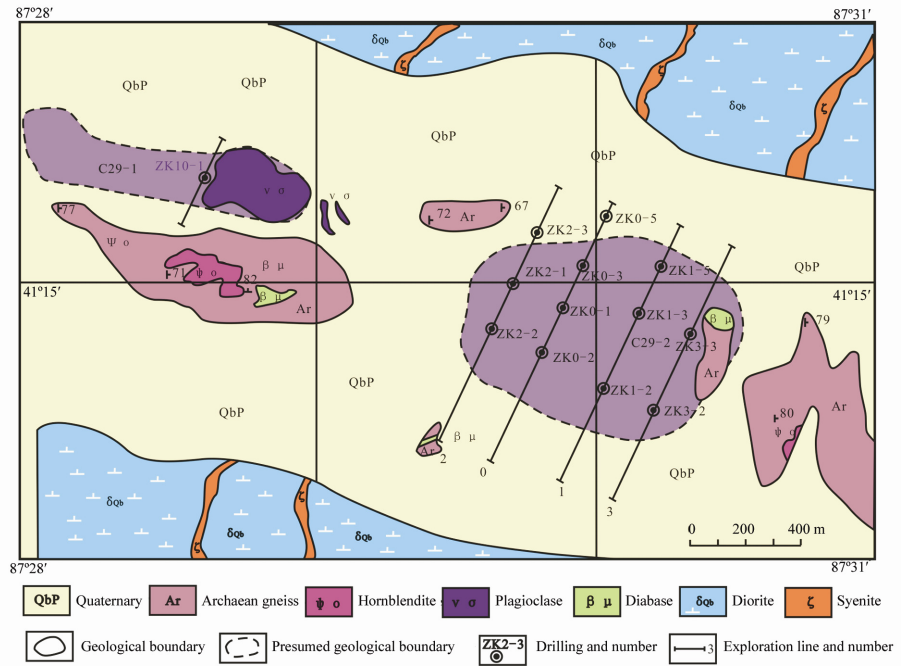

Fig. 2. Geologicalmap of the Daxigou iron-phosphous deposit in the western Kuluketage (Xia et al., 2010). It shows the locations of geo-chronological and geochemical samples.

analyses was based upon Cathodoluminescence (CL) images (Fig. 3). Zircon U-Th-Pb measurements were conducted with 32 μm diameter laser beam at the State Key Laboratory of Geological Processes and Mineral Resources, China University of Geosciences (Wuhan), using a GeoLas 2005 System. An Agilent 7700a ICP-MS instrument was used to acquire ion-signal intensities, with a 193 nm ArF-excimer laser and a homogenizing, imaging optical system (MicroLas, Göttingen, Germany). Detailed instrumentation and analytical accuracy description were given by Liu et al. (2008, 2010). Time-dependent drifts of U-Th-Pb isotopic ratios were corrected using a linear interpolation (with time) for every five analyses according to the variations of external standard zircon 91500 (i.e., 2 zircon 91500 + 5 samples + 2 zircon 91500) (Liu et al., 2010). The ages were calculated by in-house software ICPMSDataCal (ver. 9.0, China University of Geosciences) (Liu et al., 2008) and Concordia diagrams were made by Isoplot/Ex ver. 3.0 (Ludwig, 2003). Trace element compositions of zircon were calibrated against GSE-1G combined with internal standardization ^{29}Si (Liu et al., 2010).

4.2 Analysis of major and trace elements

Rock samples for analysis were carefully selected on the basis of geographical distribution, trying to represent the different rock types that occur in the area. Six samples are divided into two groups: one group includes four anorthosite samples which are none-drilling samples; the left two samples are from mineralized anorthosites which are taken from the drilling holes. All these samples were selected for major and trace element determinations. Whole-rock samples were trimmed to remove the altered surfaces, and crushed and powdered with an agate mill.

Major elements were analyzed with a PAN analytical Axios X-ray fluorescence spectrometer (XRF) from ALS Chemex (Guangzhou) Co, Ltd. A. calcined or ignited sample (0.9 g) is added to 9.0 g of Lithium Borate Flux (50%–50% $Li_2B_4O_7$–$LiBO_2$), mixed well and fused in an auto fluxer between 1050–1100℃. A flat molten glass disc was prepared from the resulting melt. This disc was then analyzed by X-ray fluorescence spectrometry. The precision of the XRF analyses at ALS Chemex was 5%.

Trace element concentrations were determined with an Elan 9000 at the same lab. A prepared sample (0.2 g) is added to lithium metaborate flux (0.9 g), mixed well and fused in a furnace at 1000℃. The resulting melt was then cooled and dissolved in 100 mL of 4% HNO_3/2% HCl_3 solution. This solution was then analyzed by inductively coupled plasma-mass spectrometry (ICP-MS). The precision of the ICP-MS analyses at ALS Chemex was better than 10% for all elements. Data for whole-rock chemistry was reported as weight percent (wt.%) and for trace-element and REE data it was reported in parts per millions (10^{-6}). The analytical results were listed in Table 2.

4.3 *In-situ* zircon Hf isotope analysis

In-situ zircon Hf isotopic analysis were conducted using a Neptune Plus MC-ICP-MS, in combination with a Geolas 2005 excimer ARF laser ablation system, at the State Key Laboratory of Geological Processes and Mineral Resources, China University of Geosciences in Wuhan, China. During the analysis, a laser repetition rate of 20 Hz at 200 mJ was used with the spot sizes of 44 μm. Details of the analytical technique used are described in Hu et al. (2012). During the analysis, the $^{176}Hf/^{177}Hf$ ratio of the standard zircon (GJ-1) was 0.282013±0.000022 (2σ, n=276), agreeing with the recommended values (Woodhead and Hergt, 2005; Wu et al., 2006; Yuan et al., 2008; Slama et al., 2008; Li et al., 2010) within 2σ error. The analytical results were listed in Table 3.

5 Analytical results

5.1 Zircon U-Pb geochronology

Zircon is relatively abundant in the anorthosite sample of DXG-16. Prior to LA-ICP-MS zircon U-Pb dating, the surfaces of the grain mounts were washed with dilute HNO_3 and pure alcohol to remove any potential lead contaminations. Zircon grains in this sample are light yellow to transparent and euhedral, and are relatively long prismatic grains with magmatogenic oscillatory zoning (Fig. 3). They have well-developed prismatic faces, while the pyramidal faces are under-developed.

They generally range up to 65–230 μm in length and 44–120 μm in width. The length/width ratios range from 1.1 to 2.5. Eighteen spot analyses were performed under a laser beam of 32 μm and all of their positions were marked on the CL images (Fig. 3). The results from the analyses were corrected according to the program of ICPMSDataCal ver. 9.0 written by Liu et al. (2008). The corrected analytical results were listed in Table 1. This table shows that the Th/U ratios of the zircon grains from these samples range from 0.39 to 1.35, and most of them are higher than 0.73. Wu and Zheng (2004) noticed that the Th/U ratios of magmatogenic zircon grains are normally higher than 0.4. Thus, the above characteristics (oscillatory zoning and Th/U ratios of 0.39 to 1.35, only one Th/U ratio is lower than 0.4) show that these zircon

grains are magmatogenic. All of the data from the spot analysis are spread along the concordia line (Fig. 4) and all fall within a narrow group ($^{206}Pb/^{238}U$ age: 1808±27 to 1834±28 Ma) and yield a weighted mean $^{206}Pb/^{238}U$ age of 1818±9 Ma (95% confidence, MSWD=0.18). The age of 1818±9 Ma is considered to represent the crystallisation age of DA.

5.2 Major elements

Representative whole-rock major and trace element compositions of DA were listed in Table 2. Among the DA samples, two samples (DXG-27 and DXG-28) are from drilling holes with their contents might being affected by mineralization, considered their high CaO and extremely low Na_2O and K_2O. In addition, some samples may have experienced some degree of alteration, such as chloritization which is the common alteration in alkaline rocks, but their LOI values (average 1.6 wt.%) are relatively low and it is believed that the alteration does not significantly affect their geochemical features.

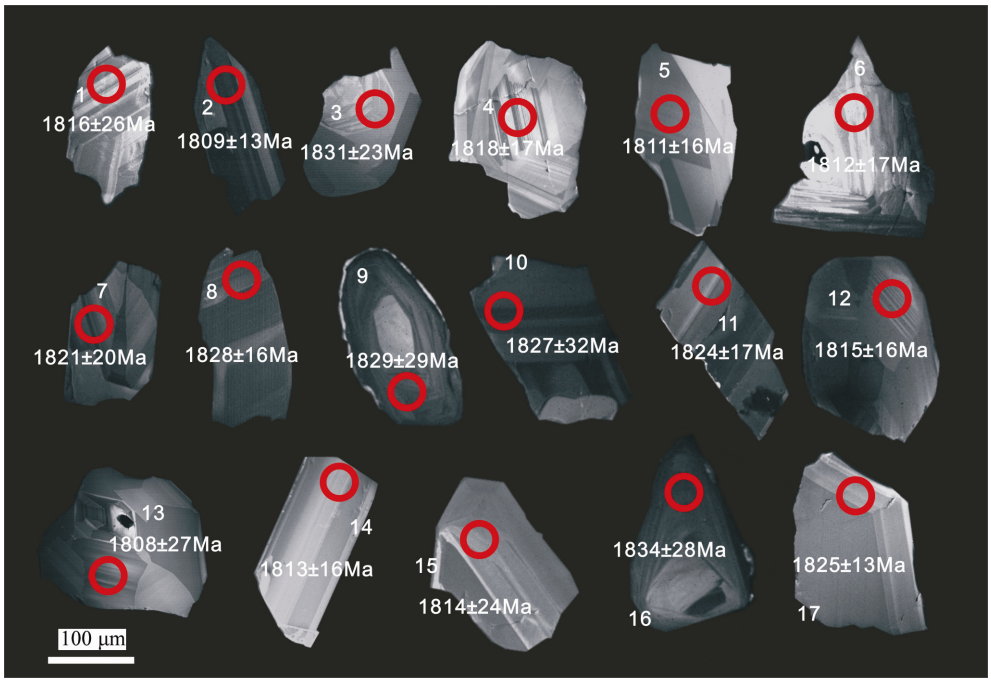

Fig. 3. CL images of zircons from the DA.

Table 1 U-Pb isotopic data of zircon from DA

Spot	Concentration (10^{-6})				U–Th–Pb isotopic ratio						Age (Ma)					
	Pb	Th	U	Th/U	$^{207}Pb/^{206}Pb$	1σ	$^{207}Pb/^{235}U$	1σ	$^{206}Pb/^{238}U$	1σ	$^{207}Pb/^{206}Pb$	1σ	$^{207}Pb/^{235}U$	1σ	$^{206}Pb/^{238}U$	1σ
DXG-16-1	37.4000	66.8000	81.9000	0.8200	0.1040	0.0042	4.6556	0.1784	0.3253	0.0054	1698	75	1759	32	1816	26
DXG-16-2	334.1000	830.5000	673.7000	1.2300	0.1059	0.0021	4.8273	0.0922	0.3240	0.0027	1731	36	1790	16	1809	13
DXG-16-3	55.4000	145.8000	108.3000	1.3500	0.1076	0.0039	4.8728	0.1641	0.3285	0.0048	1761	71	1798	28	1831	23
DXG-16-4	157.4000	352.6000	329.8000	1.0700	0.1057	0.0026	4.8063	0.1128	0.3257	0.0035	1726	45	1786	20	1818	17
DXG-16-5	267.9000	694.6000	538.8000	1.2900	0.1082	0.0026	4.9147	0.1133	0.3244	0.0032	1770	44	1805	19	1811	16
DXG-16-6	141.6000	356.9000	287.3000	1.2400	0.1093	0.0030	4.9363	0.1263	0.3246	0.0036	1788	49	1808	22	1812	17
DXG-16-7	64.6000	64.8000	156.2000	0.4100	0.1094	0.0033	4.9692	0.1498	0.3265	0.0041	1789	55	1814	25	1821	20
DXG-16-8	156.9000	362.5000	322.6000	1.1200	0.1083	0.0025	4.9621	0.1151	0.3280	0.0033	1770	43	1813	20	1828	16
DXG-16-9	27.3000	47.1000	60.7000	0.7800	0.1136	0.0052	5.0728	0.2126	0.3282	0.0059	1858	83	1832	36	1829	29
DXG-16-10	17.6000	29.2000	39.1000	0.7500	0.1140	0.0065	5.1233	0.2936	0.3276	0.0067	1865	99	1840	49	1827	32
DXG-16-11	215.1000	486.5000	452.2000	1.0800	0.1047	0.0028	4.7934	0.1258	0.3271	0.0035	1709	50	1784	22	1824	17
DXG-16-12	172.4000	264.4000	393.6000	0.6700	0.1087	0.0028	4.9509	0.1215	0.3251	0.0032	1789	46	1811	21	1815	16
DXG-16-13	29.0000	27.3000	69.9000	0.3900	0.1058	0.0048	4.7087	0.2112	0.3237	0.0055	1729	83	1769	38	1808	27
DXG-16-14	112.7000	148.5000	262.4000	0.5700	0.1069	0.0030	4.8424	0.1251	0.3247	0.0033	1747	51	1792	22	1813	16
DXG-16-15	31.0000	50.7000	69.5000	0.7300	0.1131	0.0045	5.0944	0.2000	0.3249	0.0050	1850	72	1835	33	1814	24
DXG-16-16	26.4000	57.2000	55.0000	1.0400	0.1153	0.0064	5.2668	0.2930	0.3292	0.0059	1884	100	1864	48	1834	28
DXG-16-17	450.5000	1042.2000	927.8000	1.1200	0.1050	0.0022	4.8301	0.0970	0.3273	0.0027	1715	39	1790	17	1825	13
DXG-16-18	64.4000	110.2000	143.9000	0.7700	0.1077	0.0037	4.9060	0.1583	0.3276	0.0042	1761	68	1803	27	1827	20

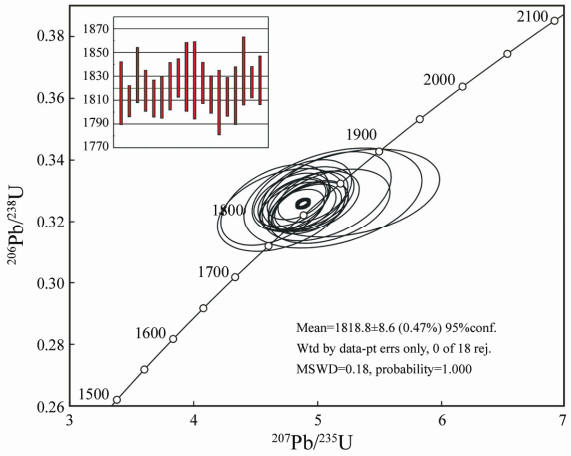

Fig. 4. U-Pb concordia of zircons from the DA.

Compared with the typical anorthosites, the rocks sampled from DA intrusive are characterized by low SiO_2 contents ranging from 42.17% to 50.8%, and high Na_2O (2.23%–5.37%), FeO (3.84%–10.89%), and TiO_2 (0.87%–6.83%) and low Al_2O_3 (12.6%–20.1%), MnO (0.07%–0.22%), and MgO (1.69%–7.6%) (Maiter, 1976). Na_2O/K_2O ratios range between 2.8 and 4.3 (average 3.5), suggesting that the rocks are relatively rich in Na. Six samples are plotted in the calc-alkaline fields in SiO_2-K_2O diagram and one sample is plotted to the high-K serious fields (Gill, 1981) (Fig. 5A). Silica alkalic indexes (δ) [$w(K_2O+Na_2O)^2$]/[$w(SiO_2–43)$] are range between 1.85–11.02 and most indexes are higher than 3.3, suggesting alkline characteristics. Except two mineralization samples, all other samples are considered as peraluminous seriously due to their A/CNK (1.24–1.61) and A/NK (2.78–4.38). These rocks are mainly plotted into the basalt and trachybasalt area from the TAS classification figure for volcanic rocks (Fig. 5B). In general, DA show similar characteristics of the major elements and samples are alkaline peraluminous basic rocks.

5.3 Trace and REE elements

Although the rare-earth elements (REE) show similar REE distribution patterns, their concentrations show small differences among the samples. The samples from the DA have ∑REE content ranging 62×10^{-6}–216×10^{-6}, LREE/HREE ratios of 9.71–13.23, and average $(La/Yb)_N$ of 20.86; while samples from the DSG have ∑REE contents ranging 15.16×10^{-6}–159×10^{-6}, LREE/HREE ratios of 4.68–14.64, and average $(La/Yb)_N$ of 13.04 (Yuan et al., to be published).

Both of these two types' samples are characterized by a certain fractionation degree of light and heavy rare earth. Average $(La/Sm)_N$ and $(Gd/Yb)_N$ of DA are 3.85 and 3.46, respectively; while the average $(La/Sm)_N$ and $(Gd/Yb)_N$ of DSG are 4.96 and 1.67, respectively. $(La/Sm)_N$ of all samples are higher than 1, showing that the LREE is moderate fractionation; while $(Gd/Lu)_N$ is higher than 1.6, showing that the HREE is also moderate fractionation.

The chondrite-normalized REE distribution patterns of the DA and DSG are similar (Fig. 6A), except for the obvious positive Eu anomaly for the one DA sample (DXG-16) and one DSG sample, and all of other samples show weak positive δEu anomaly. Additionally, DA shows relatively less positive δEu anomaly (averaging 1.21) than DSG (averaging 1.66), suggestting that magma of DA may experience the plagioclase crystallization differentiation. Despite the tiny differences in the content of ∑REE and ratio of LREE/HREE, they all display a right deviation of LREE/HREE, unconspicuous δCe.

Overall, DA and DSG have the similar characteristics of trace elements: both are rich in Pb, La and Th and depleted in Gd, Nd and Ta. In the primitive mantle (PM)-normalized spider diagram (Fig. 6B) for trace elements, the two kinds of rocks show similar distribution patterns to arc volcanic rocks (Peccerillo and Taylor, 1976; Pearce et al., 1984; Martin, 1999). Contents of Pb and La have a close positive relationship with fluid, especially when the magma source experienced fluid metasomatism which usually came from continental crust. Usually, Ti is enriched in amphibole and biotite, so the positive anomaly of Ti is resulted from the accumulation of amphibole and biotite; and negative anomaly of P has close relationship with the fractional crystallization of apatite, titanite and minerals which rich in P. Li et al. (1992) thought that orogenic type granite of continental arc have negative anomaly of Sr, P and Ti and the mature arc granite do not have the negative anomaly of Nd. DA and DSG have consistent negative anomaly of Nd and Ta, so this type of rocks may be the product of continental collision in continental arc.

5.4 *In-situ* zircon Hf isotope

Eighteen zircon samples dated by U-Pb methods were both analyzed for their Lu-Hf isotopes on the same domains, and the results were listed in Table 3. As seen from Table 3, $^{176}Lu/^{177}Hf$ ratios of most zircons are lower than 0.002, manifesting that zircons have accumulated little radiogenic Hf after they formed. Therefore $^{176}Hf/^{177}Hf$ ratios represent isotopic composition of zircons when they formed (Patchett et al., 1981; Knudsen et al., 2001; Kinny and Mass,

2003).

Eighteen spot analyses were obtained for the DA zircons, yielding variable εHf(t) values of between -6.6 and -4.43 (Table 3), one-stage model ages of 2.41–2.46 Ga and two-stage model ages of 2.63–2.74 Ga, and giving initial $^{176}Hf/^{177}Hf$ ratios ranging from 0.281452 to 0.281561. Zircons $f_{Lu/Hf}$ varies from -0.99 to -0.95, obviously lower than $f_{Lu/Hf}$ value of mafic crust (-0.34) and salic crust (-0.72) (Amelin et al., 2000). The negative εHf(t) values and Hf model ages of DA indicate that the studied rocks may be originated from the melting of the Archaean continental crust.

6 Discussion

6.1 Age of the DA

An accurate age is crucial for any discussion on the geological and genetic settings of an igneous rock. The age and patrogenesis of DA have been one of main problems since the discovery of Daxigou iron-phosphate deposit. Due to the bad natural environment, only some basic geochemistry research on anorthosite related to mineralization have been studied in this area, but little is know about the emplacement age and tectonic setting of other intrusive rocks.

Table 2 Major elements (wt.%), trace elements (10^{-6}) and rare-earth elements (10^{-6}) of the DA (1, 2, 3 samples are from Xia et al., 2010; DXG-27 and DXG-28 are collected from drilling)

Sample	DXG-2	DXG-5	DXG-16	DXG-20	DXG-27	DXG-28	1	2	3
SiO_2	48.27	45.17	42.17	50.80	50.48	49.24	47.47	48.74	49.80
Al_2O_3	16.40	18.55	16.97	20.15	13.79	13.47	12.61	18.84	16.70
FeO	7.35	6.13	9.52	3.84	1.72	1.47	10.89	4.33	7.18
Fe_2O_3	2.32	3.98	5.71	4.28	5.70	6.20	5.30	5.94	4.77
CaO	7.83	8.66	6.30	5.30	16.57	17.62	7.29	7.87	7.51
MgO	5.55	1.83	2.47	2.06	1.06	0.86	7.60	1.69	3.68
Na_2O	3.31	3.92	3.60	5.37	0.30	0.09	2.23	4.56	3.60
K_2O	1.17	0.97	0.84	1.88	0.03	0.01	0.65	1.24	1
Cr_2O_3	0.01	<0.01	0.01	<0.01	<0.01	0.01	-	-	-
TiO_2	1.27	4.51	6.83	0.87	2.26	2.84	2.34	2.60	1.63
MnO	0.14	0.07	0.12	0.09	0.06	0.08	0.22	0.087	0.14
P_2O_5	1.352	1.378	0.316	0.503	1.264	1.60	1.31	1.38	1.42
SrO	0.10	0.13	0.11	0.12	0.32	0.32	-	-	-
BaO	0.14	0.13	0.13	0.17	<0.01	0.01	-	-	-
LOI	2.68	2.04	0.98	2.15	3.13	3.21	0.91	1.303	1.65
K_2O/Na_2O	0.35	0.25	0.23	0.35	0.10	0.11	0.29	0.27	0.28
A/CNK	1.33	1.37	1.58	1.61	0.82	0.76	1.24	1.38	1.38
A/NK	3.66	3.79	3.82	2.78	41.79	134.70	4.38	3.25	3.63
Zr	43	79	139	243	266	266	110.20	110.80	156
Hf	1.30	2.30	3.60	5.60	6	5.90	-	-	-
Rb	12.6	8.50	6.60	24.50	1	0.70	-	-	-
Sr	1025	1315	1115	1100	3080	3100	684	519	873
Th	0.55	0.39	0.12	1.06	3.23	4.53	-	-	-
Nb	2.6	6.80	9.40	4.80	18.40	22.40	-	-	-
Ta	0.2	0.50	0.60	0.20	0.90	1.20	-	-	-
Ba	1320	1200	1140	1500	44	86.80	684	519	873
U	0.17	0.10	0.06	0.33	0.77	1.02	-	-	-
Pb	15	14	25	17	12	14	-	-	-
Y	21.4	16.30	5.40	21.50	35.60	40.30	13.60	15.80	15.20
La	39.6	31.60	13	43	125.50	149.50	33.40	31	39.40
Ce	88.8	71.40	25.50	87.50	247	305	68.40	62.50	82.80
Pr	11.7	9.38	3.16	10.40	29.60	36	10.90	10.60	13.40
Nd	48.3	39.40	12.50	42.40	109.50	133	37.40	36.50	45.60
Sm	8.39	7	2.14	7.38	16.90	20.70	8.48	8.96	10.40
Eu	2.78	2.62	1.53	2.47	3.73	3.87	2.42	2.12	2.54
Gd	6.29	5.08	1.60	6.74	11.65	13.95	5.54	6	6.71
Tb	0.76	0.63	0.21	0.84	1.39	1.61	0.62	1.04	1.08
Dy	4.28	3.43	1.13	4.38	7.07	8.06	3.30	3.89	4.08
Ho	0.77	0.59	0.20	0.78	1.31	1.48	0.70	0.86	0.88
Er	2.09	1.57	0.57	2.11	3.25	3.65	1.68	2.12	2.14
Tm	0.29	0.20	0.09	0.29	0.45	0.50	0.31	0.36	0.37
Yb	1.64	1.15	0.49	1.74	2.51	2.75	0.85	1.18	1.12
Lu	0.24	0.16	0.08	0.24	0.39	0.42	0.12	0.16	0.16
REE	215.93	174.21	62.2	210.27	560.25	680.49	187.72	183.09	225.88
Cl	520	160	230	-	-	-	-	-	-
F	1060	1060	380	-	-	-	-	-	-

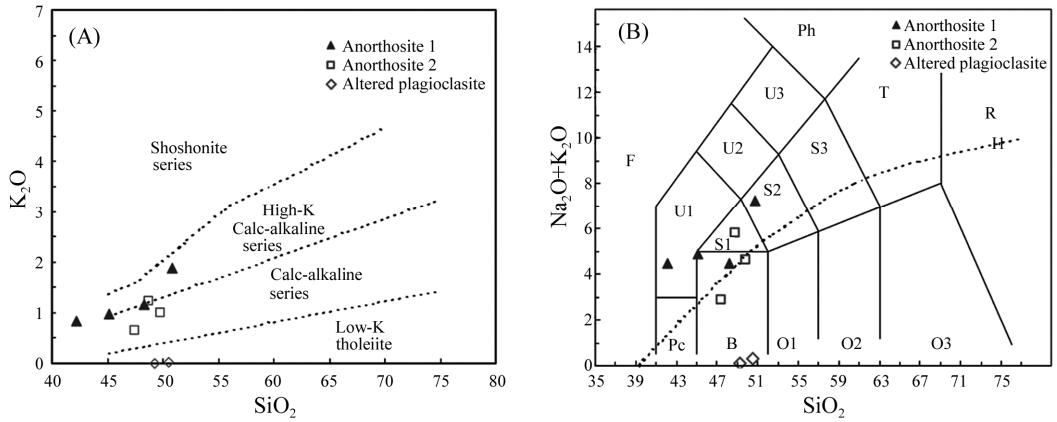

Fig. 5. Diagrams of K_2O-SiO_2 of DA (Peccerillo et al., 1976) (A) and TAS of DA (Le-Bas et al., 1986) (B).

Table 3 Lu-Hf isotopic compositions of the DA

Age (Ma)	$^{177}Hf/^{177}Hf$	1σ	$^{176}Lu/^{177}Hf$	1σ	$^{176}Yb/^{177}Hf$	1σ	εHf(0)	$f_{Lu/Hf}$	εHf(t)	T_{DM1}	T_{DM2}
1816	0.281459	0.000012	0.00019	0.000003	0.005748	0.000078	-46.44	-0.99	-6.21	2.45	2.72
1809	0.281535	0.000013	0.001524	0.000039	0.049206	0.001170	-43.75	-0.95	-5.29	2.43	2.67
1831	0.281529	0.000013	0.001138	0.000018	0.039619	0.000427	-43.95	-0.97	-4.54	2.42	2.65
1818	0.281472	0.000011	0.000394	0.000002	0.012707	0.000061	-45.99	-0.99	-5.97	2.45	2.71
1811	0.281473	0.000012	0.000599	0.000006	0.019279	0.000313	-45.95	-0.98	-6.32	2.46	2.73
1812	0.28152	0.000012	0.000789	0.000001	0.026989	0.000079	-44.28	-0.98	-4.86	2.41	2.65
1821	0.281471	0.000012	0.000202	0.000001	0.006510	0.000042	-46.01	-0.99	-5.67	2.44	2.70
1828	0.281461	0.000012	0.000238	0.000001	0.00755	0.000019	-46.36	-0.99	-5.91	2.45	2.72
1829	0.281454	0.000012	0.000186	0.000002	0.005863	0.000052	-46.60	-0.99	-6.06	2.46	2.73
1827	0.281509	0.000014	0.000697	0.000005	0.024394	0.000229	-44.65	-0.98	-4.79	2.42	2.66
1824	0.281484	0.000013	0.000357	0.000001	0.011771	0.000047	-45.55	-0.99	-5.33	2.43	2.68
1815	0.281464	0.000014	0.000312	0.000001	0.009976	0.000031	-46.26	-0.99	-6.20	2.45	2.72
1808	0.281452	0.000014	0.000168	0.000002	0.005440	0.000087	-46.68	-0.99	-6.60	2.46	2.74
1813	0.281465	0.000014	0.000172	0.000000	0.005787	0.000027	-46.20	-0.99	-6.02	2.44	2.71
1814	0.281561	0.000018	0.001653	0.000018	0.059190	0.000709	-42.84	-0.95	-4.43	2.41	2.63
1834	0.281463	0.000014	0.000348	0.000001	0.011880	0.000030	-46.27	-0.99	-5.82	2.46	2.72
1825	0.281483	0.000014	0.000442	0.000001	0.015461	0.000086	-45.58	-0.99	-5.44	2.44	2.69
1827	0.281471	0.000013	0.000261	0.000007	0.008744	0.000314	-46.02	-0.99	-5.64	2.44	2.70

As discussed earlier, the zircons of DA exhibit the oscillatory zoning and high Th/U ratios (0.39–1.35), suggesting the magmatic origin. LA-ICP-MS U-Pb dating of 18 analysis yield a weighted mean $^{206}Pb/^{238}U$ age of 1818±9 Ma, so this age is interpreted as the crystallization age of the DA rocks, which is consistent with the weighted mean $^{207}Pb/^{235}U$ age of 1830±12 Ma of DSG (Yuan et al., to be published). Combined with the similar characteristics of mineral composition (plagioclase, potassium feldspar, biotite and chlorite), geochemistry (consistent patterns of REE and trace element distribution) and isotopic age of the DA and DSG, we interpret that the crystallization age of Daxigou complex is Paleoproterozoic and the magmatic zircons indicate the magmatic origin of DXG complex, instead of metamorphic origin.

Previous researchers have made a great contribution to the tectonic evolution study on TC and adjacent areas and established the framework of the Tarim Precambrian evolution (Lu et al., 2008 a, b). A serious of high-precision dating of TC basement rocks show that it's has mainly experienced two major geological events, about 0.8–1.0 and 2.3–2.8 Ga (Zhang et al., 2012). However, recent studies indicate that the tectono-magmatic events of 1.8–2.1 Ga is also very important.

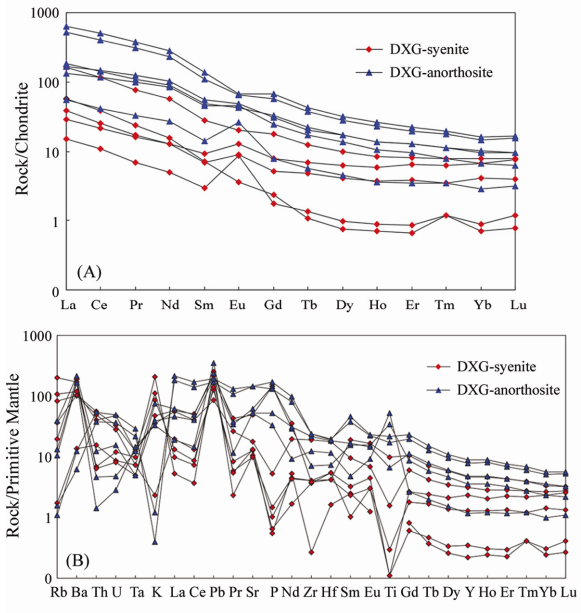

Fig. 6. ORG-normalized trace element diagram of DA (Pearce et al., 1984) (A) and chondrite-normalized REE diagram of DA (Pearce et al., 1984) (B).

In Kuruqtagh, Guo et al. (2003) identified an age of 1.8 Ga tectono-magmatic events from amphibolite in Tiemenguan area; Shu et al. (2010) conducted a LA-ICP-MS U-Pb geochronological study on detrital zircons from paragneiss and gabbro in the Quruqtagh area and found the existence of the 2.0–1.8 Ga age peaks and the corresponding tectonic-magmatic event; Wu et al. (2012) also identified a existence of the 1.85 Ga metamorphic age peaks from four metasedimentary rocks in Korla; Deng et al. (2008) obtained an age of 1916±36 Ma by LA-ICP-MS zircon U-Pb dating of several captured zircon grains from a gabbro in the Xingdi Valley of Quruqtagh; the Rb-Sr whole-rock isochron age of 2118±95 and 2067±117 Ma are respectively from the Tanzhongshan and Asigan gneissic greisen diorite (Feng et al., 1995). In addition, a lot of old zircons and inherited zircons are found in the Neoproterozoic rock and a great amount of the Paleoproterozoic metamorphic zircons or newborn metamorphic rims zircons are discovered in the Archaean gneisses. For example, Cao et al. (2010) obtained an age of 1886±61 Ma by LA-ICP-MS zircon U-Pb dating of several inherited zircon grains from the Neoproterozoic K-feldspar granite of Dapingliang plutons; Zhang et al. (2007) identified an age of 1987±20 Ma of the inherited zircon grains from diorite granite in the north of Xingdi and he also obtained the metamorphic zircon ages of 1.9–1.8 Ga from the Archaean gneiss and K-feldspar granite.

These observations, together with our new findings in this study, strongly indicate the occurrence of an important Paleoproterozoic (ca. 2.1–1.8 Ga) tectono-magmatic event in the northern TC. The age of DA (1808–1834 Ma) in the Quruqtagh area, may be an important record of tectono-magmatism during the 2.1–1.8 Ga interval.

6.2 Mantle source

DA is characterized with relatively low SiO_2, high FeO and rich in Na_2O and TiO_2, belonging to peraluminous rocks, and combined with the characteristics of U and Pb enrichment, suggesting the continental origin. The ratios of those elements, such as Nb/U and Ce/Pb, with similar total distribution coefficient, will not significantly change during partial melting or crystallization and they show similar values with their source (Cao et al., 2012). These ratios could be used to trace the source geochemistry. MORB and OIB have a Nb/U ratio of 47±10 (Hofmann, 1988), and those of primary mantle and continental crust are 34 (Sun and McDonough, 1989) and ~9.7 (Campbell, 2002), respectively. Typical mantle and crust have Ce/Pb ratios of 25±5 and lower than 15, respectively (Furman et al., 2004). The Nb/U and Ce/Pb ratios of DSG intrusive range from 14.5 to 156.6, and from 1.02 to 21.78, respectively. Generally, low Nb/U and Ce/Pb ratios may be caused by fluid metasomatism, since the fluid of the crust is rich in U and Pb and almost contains no REE (Cao et al., 2012). The existence of fluids usually increases the content of U and Pb and decreases Nb/U and Ce/Pb ratios (Chen and Han, 2006). This is also supported by the discovery of some enhydrite (e.g. biotite and hornblende) in DXG complex. The Pb content of DA (averaging 16.17×10^{-6}) is almost same of continental crust (17×10^{-6} for upper crust) (Rudnick and Gao, 2003), so the most probable source is the continental crust.

As stated above, the Hf isotopic ratio information of zircon would provide a unique *in-situ* criterion and tracer for the nature of its parent source, so it has been paid more attention (Vervoort et al., 1996; Amelin et al., 2000; Scherer et al., 2000; Griffin et al., 2002; Wu et al., 2007). Zircon is a very stable mineral and has a high closure temperature relative to other minerals. At the same time, zircon, containing 0.5% to >1% of Hf with low Lu/Hf ratios, has long been known to be excellent for the determination of Hf initial isotopic ratios (Patchett et al., 1981). According to some research, the $^{176}Lu/^{177}Hf$ ratio of zircon can represent its initial Hf isotopic composition even in granulite facies conditions, which can make zircons record the characteristics of its different magma sources. Especially by combining with zircon U-Pb dating, *in-situ* analysis of zircon Hf isotope has become more and more important for revealing crustal evolution and trace magma source (Scherer et al., 2000; Griffin et al., 2002; Wu et al., 2007).

The spots with the Paleoproterozoic ages have

high initial Hf compositions [$^{176}Hf/^{177}Hf(t)$= 0.281452–0.281561, Fig. 7A and B] with low εHf(t) values varying from -6.6 to -4.43. As shown in Fig. 8A and B, all zircons of DA show depleted mantle-like εHf(t) values, varying from -6.6 – -5.0 and all of the Hf isotope analysis of the DA fall below the chondritic uniform reservoir (CHUR) reference line and in the area of the TC. Accompany with their consistent T_{DM2} (2.63–2.74 Ga), which is exactly the same with the age of magmatitic gneiss of Archaean Tuogebulake Complex, it's reasonable to interpret that DA may be contaminated by the partial melt of the Archaean continental crust when it arise from the deep chamber.

6.3 Petrogenesis and tectonic implication of DA

6.3.1 Petrogenesis

The 1818±9 Ma zircons from DA are the first reliable crystallization age of the Paleoproterozoic intrusive rocks in Kuruqtagh block. As discussed earlier, Daxigou anorthosite belong to alkaline sodium-rich peraluminous rocks, with $w(Na_2O)/w(K_2O)>1$, high content of FeO, TiO_2 and Na_2O, low content of Al_2O_3 and CaO, and various contents of MgO, all of which exhibit the mineralogical and geochemical characteristics of volcanic anorthosite. The high LREE/HREE ratios, slightly positive Eu anomalies, high Pb, La and Th contents, low Ce, La and P contents, LILE enrichment, and HFSE (Ti, Nb and Ta) depletion all indicate that the deep basic magmas may experienced the metasomatism by the continental crust.

In the process of magma crystallization, similar elements with similar total distribution coefficient will not significantly change during partial melting or crystallization, so these elements could be used to trace the magma source. In the Rb-(Yd+Nd) diagram (Fig. 9A), both of the DA and DSG data fall in the area of the volcanic arc granite or syn-collision granite, which is consistent with continental arc source rocks that are characterized by high Yb relative to Ta (Fig. 9B).

It is generally believed that the partial melting of upper mantle plays a very important role on arc magma evolution by providing heat source and part of materials to the late magmatic rocks (Patiño, 1999; Clemens, 2003). At the same time, a large number of mafic dyke swarms suggest that Kuruqtagh block is a relatively frequently area of crust-mantle interaction. The differences in partial melting and crystallization differentiation curve indicates that the DA may be the product of repeatedly crystallization differentiation of the deep magma chamber, while the syenite granites are the result of partial melting of the upper crust, which are consistent with their geochemical characteristics.

6.3.2 Tectonic implication

In reconstructing the Neoproterozoic (1.1–0.75 Ga) supercontinental Rodinia, Hoffman (1989) recognized a more ancient Paleo-Mesoproterozoic supercontinent, based on the existence of peak ages about 1.9–1.8 Ga orogens in almost every old craton in the world (Rogers and Santosh, 2002, 2003; Zhao et al., 2002; Condie, 2002; Bleeker, 2003; Santosh et al., 2009). This Paleo-Mesoproterozoic supercontinent has been termed the 'pre-Rodinian supercontinent', 'Columbia', or 'Nuna' (e.g. Rogers, 1996; Condie, 2000, 2002; Rogers and Santosh, 2002, 2003; Zhao et al., 2002, 2004; Kusky et al., 2007).

As discussed earlier, a serious isotope age of 2.1–1.8 Ga from various areas in Kuruqtagh, together with the ca. 1.86 Ga magmatic event as documented in this study, suggest a strong ca. 1.9 Ga orogenic event in Kuruqtagh, which is also coeval with the Paleoproterozoic orogenies in other part of TC. This further conforms that the Kuruqtagh block is a part of TC in Paleoproterozoic. Together with the globally distributed 2.1–1.8 Ga crustal amalgamation events associated with the formation of the Columbia supercontinent (Condie, 2002; Rogers and Santosh, 2002; Zhao Guochun et al., 2002, 2003, 2004, 2009; Santosh et al., 2006, 2009), the Paleoproterozoic (ca. 2.1–1.8 Ga) tectono-magmatic events documented in TC were interpreted to lead to the assembly of the pre-Rodinia supercontinent-Columbia (Santosh et al., 2003, 2004; Zhao et al., 2003, 2004; and references therein for detailed discussions).

Considering the above tectonic implications, we propose the evolution process of Daxigou complex may be the following, due to the Columbia supercontinent converge, subduction oceanic crust remelt, dehydrated and lead to the partial melt of the upper mantle deed, on its gradually rise the deep magma gradually differentied, assimilated and contaminated with the middle-lower crust and firstly formed the Daxigou anorthosite; in the last, due to long-term heating of the magma activity and partial melting, the continental crust resulted of the Daxigou syenite granite.

7 Conclusions

(1) The emplacement age of Daxigou DA is 1818 ±9 Ma and the T_{DM2} of zircon Hf varies from 2.63 to 2.74 Ga, suggesting that it might experienced the magma mixing with the Archaean continental crust which is exactly outcropped in this district. Field investigation, combined with petrographic, geochronological, and geochemical evidence, shows that the Daxigou DA belongs to the Paleoproterozoic peraluminous arc-type alkaline volcanic rocks.

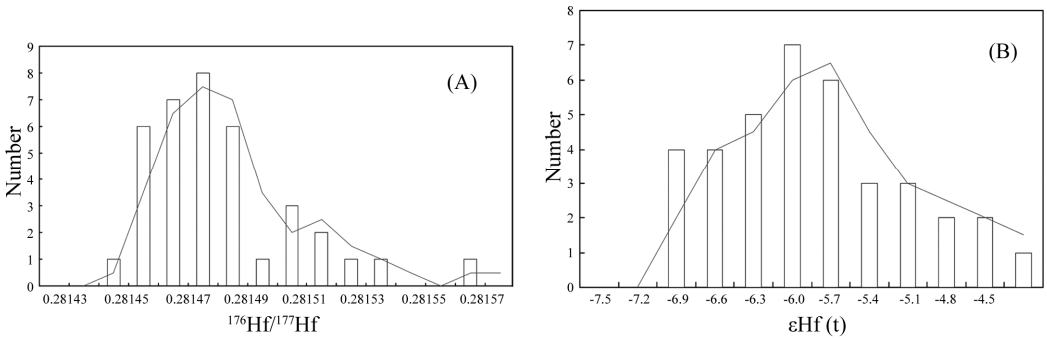

Fig. 7. εHf (t) values histograms for zircon samples (A) and initial Hf composition histograms for zircon samples (B).

Note: (1) Data for the Korla gniess are from Long et al. (2010); (2) data for the Xishankou blue quartz-bearing granitic rocks are from Lei et al., (2012).

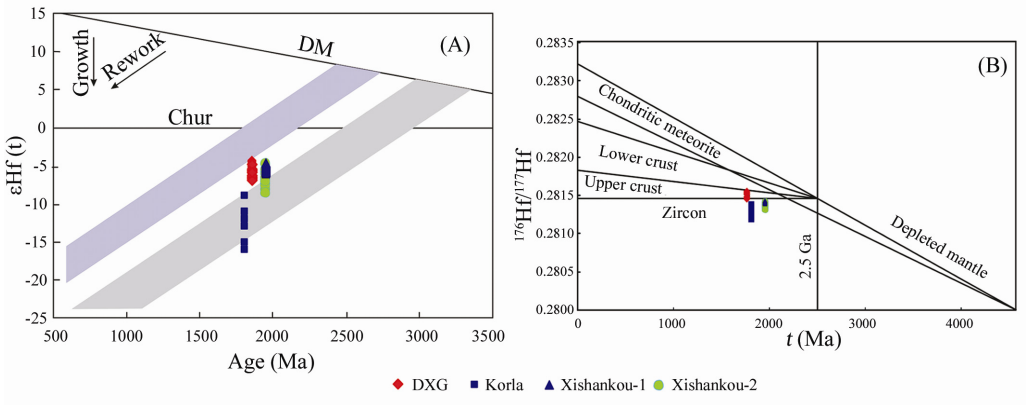

Fig. 8. Diagrams of εHf(t)-t (A) and ($^{176}Hf/^{177}Hf$)i-t of DA (B). Diagram of εHf (t) values vs. $^{206}Pb/^{238}U$ ages for zircons from the DA in the northern TC.

Note: (1) Data for the Korla gniess are from Long et al. (2010); (2) data for the Xishankou-1 and Xishankou-2 are from Lei et al. (2012).

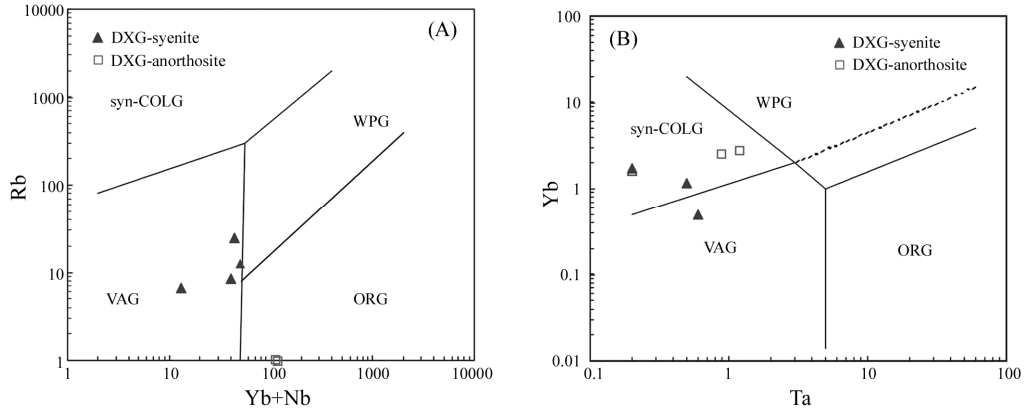

Fig. 9. (Y+Nb)–Rb discrimination diagram [Base plot is from Pearce (1996)] (A) and Ta–Yb discrimination diagram [Base plot is from Pearce (1996)] (B). VAG. Volcanic arc granite; ORG. ocean ridge granite; WPG. within-plate granite; Syn-COLG. syn-collision granite; POG. post-collision granite.

(2) The available data, together with our new findings, demonstrate that a series of the Paleoproterozoic (ca. 2.1–1.8 Ga) tectono-magmatic events occurred in the Kuruqtagh block. A continental arc-type tectonic setting is suggested for the Paleoproterozoic (ca. 1860 Ma). The Tarim Craton evidently represents a part of the assembly of the supercontinent Columbia.

(3) Due to the Columbia supercontinent converge, subduction oceanic crust remelt and dehydrated which lead to the partial melt of the upper mantle deed, on its gradually rise the deep magma gradually differentied, assimilated and contaminated with the middle-lower crust and firstly formed the Daxigou

anorthosite; in the last, due to long-term heating of the magma activity and partial melting, the continental crust resulted of the Daxigou syenite granite.

Acknowledgements We thank Zheng Han, Hu Zhaochu, Tang Wenxiu of the State Key Laboratory of Geological Processes and Mineral Resources, China University of Geosciences, Wuhan, for their assistance in LA-ICP-MS and Hf isotope determinations. All thanks to graduate students Shi Ran for their assistance during the experiment. Xi Guo-qing is thanked for help in the field work. This research was jouintly founded by the 305 Project of State Science and Technology Support Program (Grant No. 2011BAB06B04-05), the China Postdoctoral Science Foundation Funded Project (Grant No. 2012M521492 and 2013T60758), the Fundamental Research Funds for the Central Universities, China University of Geosciences (Wuhan) (Grant No. CUG120840, CUG120702 and CUGL120296).

References

Amelin Y., Lee D.C., and Halliday A.N. (2000) Early-Middle Archean crustal evolution deduced from Lu-Hf and U-Pb isotopic studies of single zircon grains [J]. *Geochimica et Cosmochimica Acta*. **64**, 4205–4225.

Bleeker W. (2003) The Late Archean record: A puzzle in ca. 35 pieces [J]. *Lithos*. **71**, 99–134.

Campbell I.H. (2002) Implications of Nb/U, Th/U and Sm/Nd in plume magma for the relationship between continental and oceanic crust formation and the depleted mantle [J]. *Geochimica et Cosmochimica Acta*. **66**, 1651–1661.

Cao Xiaofeng, Gao Xiang, Lü Xinbiao, Qin Qie, Liu Shentai, Chen Chao, Guo Ruiqing, Zhang Bin, and Hu Qitao (2012) Sm–Nd geochronology and geochemistry of a Neoproterozoic gabbro in the Kuluketage block, north-western China [J]. *International Geology Review*. **54**, 861–875.

Cao Xiaofeng, Lü Xinbiao, Lei Jianhua, Chen Chao, Wang Yuqi, Du Baofeng, Mei Wei, Gao Xiang, and Du Andao (2010) The age of the Neoproterozoic Dapingliang skarn copper deposit in Kuruketage, NW China [J]. *Resource Geology*. **60**, 397–403.

Cao Xiaofeng, Lü Xinbiao, Liu Shentai, Zhang Ping, Gao Xiang, Chen Chao, and Mo Yalong (2011) LA-ICP-MS zircon dating, geochemistry, petrogenesis and tectonic implications of the Dapingliang Neoproterozoic granites at Quruqtagh block, NW China [J]. *Precambrian Research*. **186**, 205–219.

Chen Lihui and Han Baofu (2006) Geochronology, geochemistry and Sr-Nd-Pb isotopic composition of mafic intrusive rocks in Wuqiagou area, north Xinjiang: Constraints for mantle sources and deep processes [J]. *Acta Petrologica Sinica*. **22**, 1201–1204 (in Chinese with English abstract).

Cheng Yuqi (1994) *Outline of Regional Geology in China* [M]. pp.1–517. 615 Publishing House. Beijing (in Chinese with English abstract).

Clemens J.D. (2003) S-type granitic magmas-petrogenetic issues, models and evidence [J]. *Earth-Science Reviews*. **61**, 1–18.

Condie K.C. (2000) Episodic continental growth models: Afterthoughts and extensions [J]. *Tectonophysics*. **322**, 153–162.

Condie K.C. (2002) Breakup of a Paleoproterozoic supercontinent [J]. *Gondwana Research*. **5**, 41–43.

Demoux A., Kröner A., Liu D.Y., and Badarch G. (2009) Precambrian crystalline basement in southern Mongolia as revealed by SHRIMP zircon dating [J]. *International Journal of Earth Sciences*. **98**, 1365–1380.

Deng Xingliang, Shu Liangshu, Zhu Wenbin, Ma Dongsheng, and Wang Bo (2008) Precambrian tectonism, magmatism, deformation and geochronology of igneous rocks in the Xingdi fault zone, Xinjiang [J]. *Acta Petrologica Sinica*. **24**, 2800–2808 (in Chinese with English abstract).

Feng Benzhi, Zhou Yuwen, Chi Shifu, Yang Tianqi, Zhong Chongxue, Ye Songqing, Peng Qiming, Liu Zhenghong, Jiang Qigang, and Xing Lixing (1995) *Presinian Geology, Precious and Nonferrous Metal Deposits in Kuruketage Area, Xinjiang Uygur Autonomous Region, China* [M]. pp.1–282. Geological Publishing House (Beijing). (in Chinese with English abstract).

Furman T.Y., Bryce J.G., Karson J., and Iotti A. (2004) East African rift system (EARS) plume structure: Insight from Quaternary mafic lavas of Turkana, Kenya [J]. *Journal of Petrology*. **45**, 1069–1088.

Gao Zhenjia, Chen Pulian, Lu Songnian, Peng Changwen, and Qin Zhengyong (1993) *The Precambrian Geology in Northern Xinjiang* [M]. pp.1–171. Precambrian Geology, No. 6. Geological Publishing House, Beijing (in Chinese with English abstract).

Gill J.B. (1981) *Orogenic Andesites and Plate Tectonics (Minerals and Rocks)* [M]. pp.1–100. Springer-Verlag. New York.

Griffin W.L., Wang XM, Jackson S.E., Pearson N.J., O'Reilly S.Y., Xu X.S., and Zhou X.M. (2002) Zircon chemistry and magma mixing, SE China: *In-situ* analysis of Hf isotopes, Tonglu and Pingtan igneous complexes [J]. *Lithos*. **61**, 237–269.

Guo Zhaojie, Zhang Zhicheng, Liu Shuwen, and Li Huimin (2003) U-Pb geochronological evidence for the Early Precambrian complex of the Tarim Craton, NW China [J]. *Acta Petrologica Sinica*. **19**, 537–542 (in Chinese with English abstract).

Hoffman P.F. (1989) Speculations on Laurentia's first gigayear (2.0 to 1.0 Ga) [J]. *Geology*, **17**, 135–138.

Hofmann W. (1988) Chemical differentiation of the earth: The relationship between mantle, continental crust, and oceanic crust [J]. *Earth and Planetary Science Letters*. **90**, 297–314.

Hu Aiqin and Wei Gangjian (2006) On the age of the NeoArchean Qingir gray gneisses from the northern Tarim Basin, Xinjiang, China [J]. *Acta Geologica Sinica*. **80**, 126–134 (in Chinese with English abstract).

Hu Aiqin, Wang Zhonggang, and Tu Guangchi (1997) *Geological Evolution,Petrogenesis and Metallogeny of North Xinjiang* [M]. pp.1–246. Science Press, Beijing (in Chinese with English abstract).

Hu Zhaochu, Liu Yongsheng, Gao Shan, Liu Wenqui, Zhang Wen, Tong Xirun, Lin Lin, Zong Keqing, Li Ming, Chen Haihong, Zhou Lian, and Yang Lu (2012) Improved in situ Hf isotope ratio analysis of zircon using newly designed X skimmer cone and jet sample cone in combination with the addition of nitrogen by laser ablation multiple collector ICP-MS [J]. *Journal of Analytical Atomic Spectrometry*. **27**, 1391–1399.

Kinny P.D. and Maas R. (2003) Lu-Hf and Sm-Nd isotope systems in zircon [J]. *Reviews in Mineralogy and Geochemistry*. **53**, 327–341.

Knudsen T.L., Griffin W.L., Hartz E.H., Andresen A., and Jackson S.E.

(2001) *In-situ* hafnium and lead isotope analyses of detrital zircons from the Devonian sedimentary basin of NE Greenland: A record of repeated crustal reworking [J]. *Contributions to Mineralogy and Petrology*. **141**, 83–94.

Kusky T.M., Li Jianghai, and Santosh M. (2007) The Paleoproterozoic North Hebei Orogen: North China craton's collisional suture with the Columbia supercontinent [J]. *Gondwana Research*. **12**, 4–28.

Le-Bas M.J., Le-Maitre R.W., Streckeisen A., and Zanettin B. (1986) A chemical classification of volcanic rocks based on the total alkali silica diagram [J]. *Journal of Petrology*. **27**, 745–750.

Lei Ruxiong, Wu Changzhi, Chi Guoxiang, Chen Gang, Gu Liangxing, and Jiang Yaohui (2012) Petrogenesis of the Palaeoproterozoic Xishankou pluton, northern Tarim block, Northwest China: Implications for assembly of the supercontinent Columbia [J]. *International Geology Review*. **54**, 1829–1842.

Li Changnian (1992) *Peterology of Trace Element of Igneous* [M]. pp.1–195. China University of Geosciences Press, Wuhan (in Chinese with English abstract).

Li Quan, Yu Haifeng, and Xiu Qunye (2002) On Precambrian basement of the eastern Tianshan Mountains, Xinjiang [J]. *Xinjiang Geology*. **20**, 346–351 (in Chinese with English abstract).

Li Xianhua, Long Wengguo, Li Qiuli, Liu Yu, Zheng Yongfei, Yang Yueheng, Chamberlain K.R., Wan Defang, Guo Cunhua, Wang Xuance, and Tao Hua (2010) Penglai zircon megacryst: A potential new working reference for microbeam analysis of Hf-O isotopes and U-Pb age [J]. *Geostandards and Geoanalytical Research*. **34**, 117–134.

Liu Yongsheng, Gao Shan, Hu Zhaochu, Gao Gao Changgui, Zong Keqing, and Wang Dongbing (2010) Continental and oceanic crust recycling-induced melt-peridotite interactions in the Trans-North China Orogen: U–Pb dating, Hf isotopes and trace elements in zircons of mantle xenoliths [J]. *Journal of Petrology*. **51**, 537–571.

Liu Yongsheng, Hu Zhaochu, Gao Shan, Günther D., Xu Juan, Gao Changgui, and Chen Haihong (2008) In situ analysis of major and trace elements of anhydrous minerals by LA-ICP-MS without applying an internal standard [J]. *Chemical Geology*. **257**, 34–43.

Long Xiaoping, Yuan Chao, Sun Min, Zhao Guochun, Xiao Wenjiao, Wang Yujing, Yang Yueheng, and Hu Aiqin (2010) Archean crustal evolution of the northern Tarim craton, NW China: Zircon U–Pb and Hf isotopic constraints [J]. *Precambrian Research*. **180**, 272–284.

Lu Songnian (1992) *Geological Evolution of Proterozoic in Kuruketage, Xinjiang* [M]. pp. 279–292. Bulletin of the Tianjin Institute of Geology and Mineral Resources, CAGS (in Chinese with English abstract).

Lu Songnian, Li Huaikun, Zhang Chuanlin, and Niu Guanghua (2008a) Geological and geochronological evidence for the Precambrian evolution of the Tarim Craton and surrounding continental fragments [J]. *Precambrian Research*. **160**, 94–107.

Lu Songnian, Zhao Guochun, Wang Huichu, and Hao Guojie (2008b) Precambrian metamorphic basement and sedimentary cover of the North China Craton: A review [J]. *Precambrian Research*. **160**, 77–93.

Ludwig K.R. (2003) Isoplot 3.0-A geochronological toolkit for Microsoft Excel [J]. *Berkeley Geochronology Center Special Publication*. **4**, 70.

Luo Xinrong, Shi Fuping, Fan Weidong, and Luo Xintao (2007) Age and geochemistry of Neoproterozoic granite from Kuruketage in the north of Tarim, Xinjiang [J]. *Resources Survey and Environment*. **28**, 235–241 (in Chinese with English abstract).

Martin H. (1999) Adakitic magmas: Modern analogues of Archaean granitoids [J]. *Lithos*. **46**, 411–429.

Patchett P.J., Kouvo O., Hedge C.E., and Tatsumoto M. (1981) Evolution of continental crust and mantle heterogeneity: Evidence from Hf isotopes [J]. *Contributions to Mineralogy and Petrology*. **78**, 279–297.

Patiño D.A.E. (1999) What do experiments tell us about the relative contributions of crust and mantle to the origins of granitic magmas? In *Understanding Granites. Intergrating New and Classical Techniques* (eds. Castro A., Fernandes C., and Vigene**re**sse J.L.) [M]. The Geological Society of London. **168**, 55–75.

Pearce J., Harris N.B.W., and Tindle A.G. (1984) Trace element discrimination diagrams for the tectonic interpretation of granitic rocks [J]. *Journal of Petrology*. **25**, 956–983.

Pearce J.A. (1996) Sources and settings of granitic rocks [J]. *Episodes*. **19**, 120–125.

Peccerillo A. and Taylor S.R. (1976) Geochemistry of Eocene calc-alkaline volcanic rocks from the Kastamounu area, northern Turkey [J]. *Contributions to Mineralogy and Petrology*. **58**, 63–81.

Rogers J.J.W. (1996) A history of continents in the past three billion years [J]. *Journal of Geology*. **104**, 91–107.

Rogers J.J.W. and Santosh M. (2002) Configuration of Columbia, a Mesoproterozoic supercontinent [J]. *Gondwana Research*. **5**, 5–22.

Rogers J.J.W. and Santosh M. (2003) Supercontinent in earth history [J]. *Gondwana Research*. **6**, 357–368.

Rudnick R.L. and Gao Shan (2003) *Composition of the Continental Crust* (eds. Hollan H.D. and Turekin K.K.) [M]. pp.1–64. Treatise on geochemistry. Oxford, Elsevier.

Santosh M., Sajeev K., and Li Jianghai (2006) Extreme crustal metamorphism during Columbia supercontinent assembly: Evidence from North China Craton [J]. *Gondwana Research*. **10**, 256–266.

Santosh M., Wan Yusheng, Liu Dunyi, Dong Chunyan, and Li Jianghai (2009) Anatomy of zircons from an ultrahot orogen: The amalgamation of the North China Craton within the Supercontinent Columbia [J]. *Journal of Geology*. **117**, 429–443.

Santosh M., Yokoyama K., and Acharyya S.K. (2004) Geochronology and tectonic evolution of Karimnagar and Bhopalpatnam granulite belts, central India [J]. *Gondwana Research*. **7**, 501–518.

Santosh M., Yokoyama K., Biju-Sekhal S., and Rogers J.J.W. (2003) Multiple tectonothermal events in the granulite blocks of southern India revealed from EPMA dating: Implications on the history of supercontinents [J]. *Gondwana Research*. **6**, 29–63.

Scherer E.E., Cameron K.L., and Blichert-Toft J. (2000) Lu-Hf garnet geochronology: Closure temperature relative to the Sm-Nd system and the effects of trace mineral inclusions [J]. *Geochimica et Cosmochimica Acta*. **64**, 3413–3432.

Shu Liangshu, Deng Xingliang, Zhu Wenbin, Ma Dongsheng, and Xiao Wenjiao (2010) Precambrian tectonic evolution of the Tarim block, NW China: New geochronological insights from the Quruqtagh domain [J]. *Journal of Asian Earth Sciences*. **41**, 774–782.

Slama J., Kosler J., Condon D.J., Crowley J.L., Gerdes A., Hanchar J.M., Horstwood M.S.A., Morris G.A., Nasdala L., Norberg N., Schaltegger U., Schoene B., Tubrett M.N., and Whitehouse M.J. (2008) Zircon—A new natural reference material for U–Pb and Hf isotopic microanalysis [J]. *Chemistry Geology*. **249**, 1–35.

Sun Baosheng and Huang Jianhua (2007) Sm-Nd isotopic age of Qieganbulak ultrabasic-carbonatite complex in Xinjiang, China and its geological significance [J]. *Acta Petrologica Sinica*. **23**, 1611–1616 (in Chi-

nese with English abstract).

Sun S.S. and McDonough W.F. (1989) Chemical and isotopic systematics of oceanic basalt: Implication for mantle composition and processes. In *Magmatism in the Ocean Basin* (eds. Saunders A.D., and Morry M.J.) [M]. London, Geological Society of Special Publication. **42**, 528–548.

Vervoort J.D., Pachett P.J., Gehrels G.E., and Nutman A.P. (1996) Constraints on early earth differentiation from hafnium and neodymium isotopes [J]. *Nature*. **379**, 624–627.

Wang Hongliang, Xu Xueyi, He Shiping, and Chen Juanlu (2007) *Map of Tianshan and Adjacent Area (1:1000000)* [Z]. Geology Publishing House, Beijing (in Chinese with English abstract).

Woodhead J.D. and Hergt J.M. (2005) A preliminary appraisal of seven natural zircon reference materials for *in-situ* Hf isotope determination [J]. *Geostandards and Geoanalytical Research*. **29**, 183–195.

Wu Fuyuan, Li Xianhua, Zheng Yongfei, and Gao Shan (2007) Lu-Hf isotopic systematics and their applications in petrology [J]. *Acta Petrologica Sinica*. **23**, 185–220 (in Chinese with English abstract).

Wu Fuyuan, Yang Yueheng, Xie Liewen, Yang Jinhui, and Xu Ping (2006) Hf isotopic compositions of the standard zircons and baddeleyites used in U–Pb geochronology [J]. *Chemistry Geology*. **234**, 105–126.

Wu Hailin, Zhu Wenbin, Shu Liangshu, Zheng Bihai, He Jingwen, and Luo Meng (2012) Records of the assemblage event of Columbia supercontinent in the northern Tarim Craton [J]. *Geological Journal of China Universities*. **18**, 686–700 (in Chinese with English abstract).

Wu Yuanbao and Zheng Yongfei (2004) Study on the genesis of zircon and its restrictions on explaining the U-Pb age [J]. *Chinese Science Bulletin*. **49**, 1589–1604 (in Chinese with English abstract).

Xia Xuehui, Yuan Jiazhong, Xi Guoqing, and Liang Zhongpeng (2010) Geochemistry of complex rocks and characteristics of Daxigou iron-phosphorite deposits, Xinjiang [J]. *Journal of Jilin University* (Earth Science Edition). **40**, 879–886 (in Chinese with English abstract).

Xiao Wenjiao and Kusky T. (2009) Geodynamic processes and metallogenesis of the Central Asian and related orogenic belts: Introduction [J]. *Gondwana Research*. **16**, 167–169.

Xu Bei, Jiang Ping, Zheng Haifei, Zou Haibo, Zhang Lifei, and Liu Dunyi (2005) U–Pb zircon geochronology and geochemistry of Neoproterozoic volcanic rocks in the Tarim Block of Northwest China: Implications for the breakup of Rodinia supercontinent and Neoproterozoic glaciations [J]. *Precambrian Research*. **136**, 107–123.

Xu Bei, Kou Xiaowen, Song Biao, Wei Wei, and Wang Yu (2008) SHRIMP dating of the Upper Proterozoic volcanic rocks in the Tarim plate and constraints on the Neoproterozoic glaciation [J]. *Acta Petrologica Sinica*. **24**, 2857–2862 (in Chinese with English abstract).

Xu Bei, Xiao Shuhai, Zou Haibo, Chen Yan, Li Zhengxiang, Song Biao, Liu Dunyi, Zhou Chuanming, and Yuan Xunlai (2009) SHRIMP zircon U–Pb age constraints on Neoproterozoic Quruqtagh diamictites in NW China [J]. *Precambrian Research*. **168**, 247–258.

Yuan Honglin, Gao Shan, Dai Mengning, Zong Chunlei, Gunther D., Fontaine G.H., Liu Xiaoming, and Diwu Chunrong (2008) Simultaneous determinations of U–Pb age, Hf isotopes and trace element compositions of zircon by excimer laser-ablation quadrupole and multiple-collector ICP-MS [J]. *Chemistry Geology*. **247**, 100–118.

Zhang Chuanlin, Li Huaikun, and Wang Hongyan (2012) A review on precambrian tectonic evolution of Tarim Block: Possibility of interaction between Neoproterozoic plate subduction and mantle plume [J]. *Geological Review.* **58**, 923–933 (in Chinese with English abstract).

Zhang Chuanlin, Li Zhengxiang, Li Xianhua, and Ye Haiming (2009) Neoproterozoic mafic dyke swarm in north margin of the Tarim, NW China: Age, geochemistry, petrogenesis and tectonic implications [J]. *Journal of Asian Earth Sciences*. **35**, 167–179.

Zhang Chuanlin, Lu Songnian, Yu Haifeng, and Ye Haiming (2007b) Tectonic evolution of western orogenic belt: evidences from zircon SHRIMP and LA-ICP-MS U–Pb ages [J]. *Science in China* (D-series). **50**, 1–12 (in Chinese with English abstract).

Zhang Chuanlin, Yang Dongsheng, Wang Hongyan, Takahashi Y., and Ye Haiming (2011) Neoproterozoic mafic-ultramafic layered intrusion in Quruqtagh of northeastern Tarim block, NW China: Two phases of mafic igneous with different mantle sources [J]. *Gondwana Research*. **19**, 177–190.

Zhang Chuanlin, Yu Haifeng, and Ye Haiming (2007c) Discussions on the Neoproterozoic diorites in central Tarim Basin: A comment on "Geochronology and geochemistry of deepdrill-core samples from the basement of the central Tarim basin" [J]. *Journal of Asian Earth Sciences*. **29**, 177–180.

Zhang Chuanlin, Li Xianhua, Li Zhengxiang, Lu Songnian, Ye Haimin, and Li Huimin (2007a) Neoproterozoic ultramafic-mafic-carbonatite complex and granitoids in Quruqtagh of northeastern Tarim block, western China: Geochronology, geochemistry and tectonic implications [J]. *Precambrian Research*. **152**, 149–169.

Zhao Guochun, Cawood P.A., Wilde S.A., and Sun Min (2002) Review of global 2.1–1.8 Ga orogens: Implications for a pre-Rodinia supercontinent [J]. *Earth-Science Reviews*. **59**, 125–162.

Zhao Guochun, He Yanhong, and Sun Min (2009) The Xiong'er volcanic belt at the southern margin of the North China Craton: Petrographic and geochemical evidence for its outboard position in the Paleo-Mesoproterozoic Columbia Supercontinent [J]. *Gondwana Research*. **16**, 170–181.

Zhao Guochun, Sun Min, Wilde S.A., and Li Sanzhong (2003) Assembly, accretion and breakup of the Paleo-Mesoproterozoic Columbia supercontinent: Records in the North China Craton [J]. *Gondwana Research*. **6**, 417–434.

Zhao Guochun, Sun Min, Wilde S.A., and Li Sanzhong (2004) A Paleo-Mesoproterozoic supercontinent: Assembly, growth, and breakup [J]. *Earth-Science Reviews*. **67**, 91–123.

Zhu Wenbin, Zhang Zhiyong, Shu Liangshu, Lu Huafu, Sun Jinbao, and Yang Wei (2008) SHRIMP U–Pb zircon geochronology of Neoproterozoic Korla mafic dykes in the northern Tarim block, NW China: Implications for the long-lasting breakup process of Rodinia [J]. *Journal of the Geological Society, London*. **165**, 887–890.